


## Nonthermal vibrations in biased molecular junctions

Tao Wang, Lei-Lei Nian,<sup>\*</sup> and Jing-Tao Lü<sup>†</sup>

*School of Physics and Wuhan National High Magnetic Field Center, Huazhong University of Science and Technology, Wuhan 430074, People's Republic of China*

 (Received 21 March 2020; accepted 26 July 2020; published 18 August 2020)

We study vibrational statistics in current-carrying model molecular junctions using a master equation approach. In particular, we concentrate on the validity of using an effective temperature  $T_{\text{eff}}$  to characterize the nonequilibrium steady state of a vibrational mode. We identify cases in which a single  $T_{\text{eff}}$  cannot fully describe one vibrational state. In such cases, the probability distribution among different vibrational states does not follow the Boltzmann type. Consequently, the actual entropy (free energy) of the vibrational mode is lower (higher) than the corresponding thermal value given by  $T_{\text{eff}}$ , indicating extra work can be extracted from these states. Our results will be useful for the study of a nonthermal vibrational state in the thermodynamics of nanoscale systems, and its usage in nanoscale heat engines.

DOI: [10.1103/PhysRevE.102.022127](https://doi.org/10.1103/PhysRevE.102.022127)

### I. INTRODUCTION

In recent years, electron transport through a single molecular junction has received considerable attention both experimentally and theoretically in view of its importance in molecular electronics [1–6]. Many techniques have been developed to couple a single molecule to two electrodes, and to measure its electrical conductance [7–10]. The conductance is not only affected by the molecule in the junction, but also by the coupling between the molecule and the electrodes, the electric structure of the electrodes, and the interaction between electrons and molecular vibrations [11]. The vibrations can be excited when the applied voltage bias exceeds the molecular vibrational energy. Thus, energy transfer from the electronic to the vibrational degrees of freedom takes place, resulting in energy accumulation in the vibrational system and resultant heat transport [12–17]. This is loosely termed Joule heating, although deterministic energy transfer through work may take place simultaneously [18–20]. This may in turn lead to the conformation change and atomic rearrangements [21,22]. In the extreme case, the molecular junction can be destroyed through breaking of a chemical bond. On the other hand, through specially designed electronic structure, one may use the nonequilibrium effect to cool the molecular junctions, leading to current-induced cooling [23–27].

The concept of effective temperature has been used both theoretically and experimentally to describe the junction heating and cooling when it reaches the nonequilibrium steady state under applied voltage bias [11,28–32]. The purpose of this work is to show that this is not always the case. We illustrate the nonthermal statistical properties of the vibrations by considering two model systems that have been widely used in previous studies. In the first model, we consider a vibrational laser where one vibrational mode couples to two

electronic states via the Su-Schrieffer-Heeger-like coupling [25,33–35]. In the second model, we consider Holstein-type on-site coupling between one electronic state with one vibrational mode [36–38]. In both models, we find situations in which one effective temperature is not enough to describe the statistical properties of the vibrational mode.

### II. MODELS AND METHODS

#### A. Model I: A two-level molecular junction

The first model we consider is a molecular junction consisting of two levels coupled to electrodes as depicted in Fig. 1(a). The vibrational mode can be excited by the inelastic transitions between two electronic states. The corresponding Hamiltonian is

$$\begin{aligned}
 \mathcal{H} &= \mathcal{H}_m + \mathcal{H}_{\text{el}} + \mathcal{H}_{ep} + \mathcal{H}_p + \mathcal{H}_b, \\
 \mathcal{H}_m &= \sum_{i=1,2} \varepsilon_i n_i + U_{12} n_1 n_2, \\
 \mathcal{H}_{\text{el}} &= \sum_{\alpha=L,R} \sum_k (\varepsilon_{k\alpha} - \mu_\alpha) c_{k\alpha}^\dagger c_{k\alpha} \\
 &\quad + \sum_{\alpha=L,R} \sum_k \sum_{i=1,2} (V_{\alpha k,i} c_{k\alpha}^\dagger d_i + \text{H.c.}), \\
 \mathcal{H}_{ep} &= m_{ep} (a_p^\dagger d_1^\dagger d_2 + a_p d_2^\dagger d_1), \\
 \mathcal{H}_p &= \hbar\omega_p \left( a_p^\dagger a_p + \frac{1}{2} \right), \\
 \mathcal{H}_b &= \sum_\alpha \hbar\omega_\alpha \left( a_\alpha^\dagger a_\alpha + \frac{1}{2} \right) + \sum_\alpha t_{\alpha p} (a_\alpha^\dagger + a_\alpha) (a_p^\dagger + a_p),
 \end{aligned} \tag{1}$$

where  $\mathcal{H}_m$  is the Hamiltonian of the molecule,  $n_i = d_i^\dagger d_i$  is the electron number operator for state  $i$ ,  $\varepsilon_i$  is the corresponding energy, and  $U_{12}$  is the intersite Coulomb charging energy. The two electrodes and their coupling with the molecule are described by  $\mathcal{H}_{\text{el}}$ .  $c_{k\alpha}^\dagger$  ( $c_{k\alpha}$ ) is the creation (annihilation)

<sup>\*</sup>llnian@hust.edu.cn

<sup>†</sup>jtl@hust.edu.cn

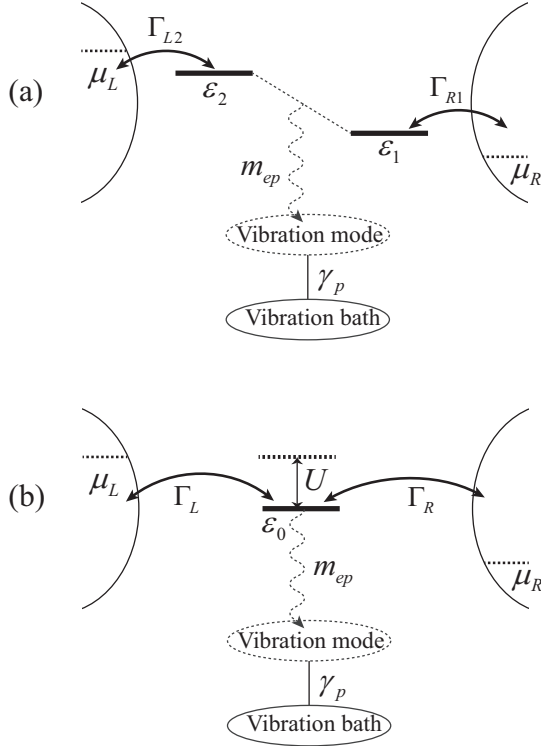


FIG. 1. (a) Schematic model of the transport in a bias-driven single molecular junction. The molecule consisting of two levels  $\varepsilon_1$  and  $\varepsilon_2$  is coupled to two electrodes ( $L$  and  $R$ ) characterized by energy-independent parameters  $\Gamma_{L2}$  and  $\Gamma_{R1}$ . The vibrational mode can be excited due to electron-vibration  $m_{ep}$  when the bias voltage ( $eV_{\text{bias}} = \mu_L - \mu_R$ ) between electrodes is large than the energy of the mode. The statistics of the vibrational mode can be obtained from the bath with a dissipation ratio  $\gamma_p$ . (b) Schematic representation of a single-level molecular junction similar to (a). Here, the vibrational excitation is caused by the Holstein-type on-site coupling between one electronic state  $\varepsilon_0$  with Coulomb interaction  $U$ .

operator of an electron with the wave vector  $k$  in the electrode  $\alpha$ .  $\varepsilon_{k\alpha}$  and  $\mu_\alpha$  are the corresponding energy and the chemical potential, respectively.  $V_{\alpha k, i}$  is the electrode-molecule coupling parameter. The electronic states couple to a vibrational mode,  $\mathcal{H}_{ep}$  is the corresponding Hamiltonian, and the vibrational mode is described by  $\mathcal{H}_p$ . The last term  $\mathcal{H}_b$  describes damping of the vibrational mode due to coupling to a vibrational bath.  $a_p^\dagger$  ( $a_p$ ) and  $a_\alpha^\dagger$  ( $a_\alpha$ ) are the creation (annihilation) operators of the vibrational mode and the bath with angular frequencies  $\omega_p$  and  $\omega_\alpha$ , with  $t_{\alpha p}$  being their coupling.

To study the vibration statistics, we use the master equation approach of the Lindblad form. The molecule-electrode coupling is regarded as a perturbation [39,40]. We furthermore consider the molecule system in the strong Coulomb blockade regime ( $U_{12} \rightarrow \infty$ ), that is, only the occupation by a single excess electron is allowed. Then, the effective Hilbert space of the molecular system is spanned by three states, which are  $|0\rangle = |0, 0\rangle$ ,  $|a\rangle = |1, 0\rangle$ , and  $|b\rangle = |0, 1\rangle$ . Meanwhile, we can define creation operators of the ground and excited states for the molecule as  $d_g^\dagger = |a\rangle\langle 0|$  and  $d_e^\dagger = |b\rangle\langle 0|$  with energies  $\varepsilon_1$  and  $\varepsilon_2$ , respectively. The Hamiltonian in Eq. (1) can be rewritten in such a representation. Under the

Born-Markov approximation, the reduced density matrix for the electron-vibration system follows the following equation of motion:

$$\dot{\rho} = \frac{1}{i\hbar}[\mathcal{H}_0, \rho] + \mathcal{L}_{\text{el}}[\rho] + \mathcal{L}_p[\rho], \quad (2)$$

with  $\mathcal{H}_0 = \mathcal{H}_m + \mathcal{H}_p + \mathcal{H}_{ep}$ . The first term on the right-hand side describes the quantum coherent evolution of the electron-vibration system. The last two terms correspond to the dissipation of the system due to the interaction with electrodes and the vibrational bath. We have

$$\begin{aligned} \mathcal{L}_{\text{el}}[\rho] = & \frac{1}{2} \sum_{\alpha} \Gamma_{\alpha 1} \{f_{\alpha}(\varepsilon_g) \mathcal{D}[d_g, \rho] + [1 - f_{\alpha}(\varepsilon_g)] \mathcal{D}[d_g^\dagger, \rho]\} \\ & + \frac{1}{2} \sum_{\alpha} \Gamma_{\alpha 2} \{f_{\alpha}(\varepsilon_e) \mathcal{D}[d_e, \rho] \\ & + [1 - f_{\alpha}(\varepsilon_e)] \mathcal{D}[d_e^\dagger, \rho]\}, \end{aligned} \quad (3)$$

where  $\Gamma_{\alpha i}(\varepsilon) = 2\pi \sum_k |V_{\alpha k, i}|^2 \delta(\varepsilon - \varepsilon_{k\alpha})$  is the level broadening function of the state  $i$  due to coupling with electrode  $\alpha$ . We have ignored its energy dependence here. The Lindblad superoperators act according to  $\mathcal{D}[\mathcal{A}, \rho] = 2\mathcal{A}^\dagger \rho \mathcal{A} - \{\mathcal{A}\mathcal{A}^\dagger, \rho\}$ . For the vibration,  $\mathcal{L}_p[\rho]$  can be written as

$$\mathcal{L}_p[\rho] = \frac{\gamma_p}{2} (1 + n_B) \mathcal{D}[a_p^\dagger, \rho] + \frac{\gamma_p}{2} n_B \mathcal{D}[a_p, \rho], \quad (4)$$

where  $\gamma_p(\omega) = 2\pi \sum_{\alpha} |t_{\alpha p}|^2 \delta(\omega - \omega_{\alpha})$  characterizes the coupling to the vibrational bath.  $n_B = [e^{\hbar\omega_p/k_B T} - 1]^{-1}$  is the average occupation of the vibrational mode  $\omega_p$  in equilibrium state at temperature  $T$ .

Using the standard quantum master equation procedure, the time evolution of the vibrational density matrix element can be written as

$$\begin{aligned} \frac{dp_{m,n}}{dt} = & -i\omega_p(m-n)p_{m,n} - im_{ep}[\sqrt{m+1}\rho_{m+1,n}^{ge} \\ & - \sqrt{n+1}\rho_{m,n+1}^{eg} + \sqrt{m}\rho_{m-1,n}^{eg} - \sqrt{n}\rho_{m,n-1}^{ge}] \\ & + \frac{\gamma_p}{2} [2(n_B+1)\sqrt{(m+1)(n+1)}p_{m+1,n+1} \\ & - (n_B+1)(m+n)p_{m,n} \\ & + 2n_B\sqrt{mn}p_{m-1,n-1} - n_B(m+n+2)p_{m,n}], \end{aligned} \quad (5)$$

where the combined density matrix elements  $\rho_{mn}^{ge}$  and  $\rho_{mn}^{eg}$  are given in Appendix A. For  $m = n$ ,  $p_{m,m}$  describes the probability of finding  $m$  vibrational quanta.

## B. Model II: A single-level molecular junction

A single-level model in Fig. 1(b) is considered in this case. The corresponding Hamiltonian is

$$\begin{aligned} \mathcal{H} = & \mathcal{H}_m + \mathcal{H}_{\text{el}} + \mathcal{H}_{ep} + \mathcal{H}_p + \mathcal{H}_b, \\ \mathcal{H}_m = & \varepsilon_0 n + U n(n-1), \\ \mathcal{H}_{\text{el}} = & \sum_{\alpha=L,R} \sum_k (\varepsilon_{k\alpha} - \mu_\alpha) c_{k\alpha}^\dagger c_{k\alpha} \\ & + \sum_{\alpha=L,R} \sum_k \sum_{i=\uparrow,\downarrow} (V_{\alpha k, i} c_{k\alpha}^\dagger d_i + \text{H.c.}), \\ \mathcal{H}_{ep} = & m_{ep} (a_p^\dagger + a_p) n, \end{aligned} \quad (6)$$

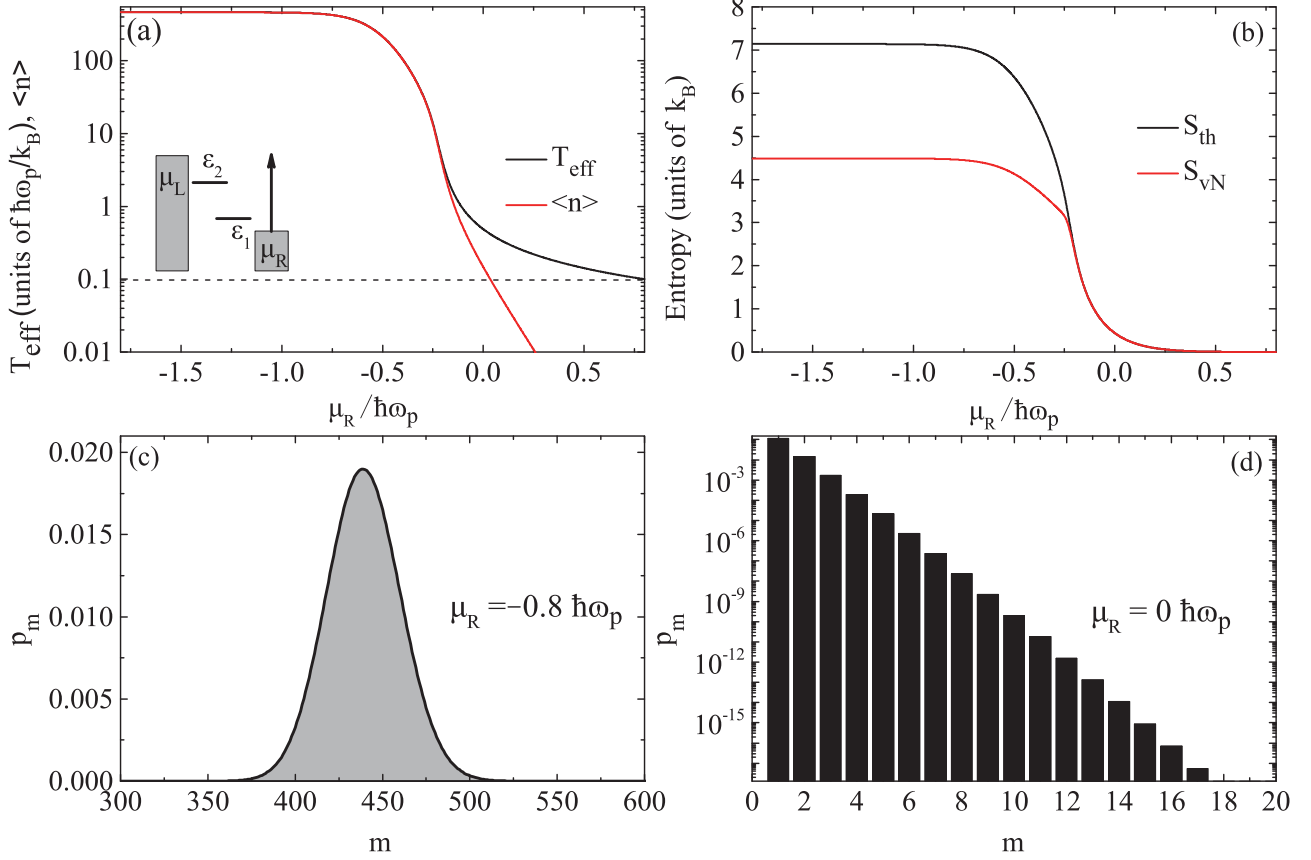


FIG. 2. (a) The effective temperature  $T_{\text{eff}}$  and the average population  $\langle n \rangle$  as a function of the chemical potential of the right electrode  $\mu_R$  with  $\mu_L = 0.8 \hbar\omega_p$ . The inset shows two molecular levels  $\varepsilon_1$  and  $\varepsilon_2$  coupled to two electrodes with chemical potentials  $\mu_L$  and  $\mu_R$ , where  $\mu_R$  increases in the direction of the arrow. (b) Entropy  $S_{\text{th}}$  and  $S_{\text{vN}}$  vs  $\mu_R$ . (c) and (d) Vibration statistics at  $\mu_R = 0.8 \hbar\omega_p$  and  $\mu_R = 0 \hbar\omega_p$ , respectively. The other parameters are  $\Gamma_{L2} = 0.01 \hbar\omega_p$ ,  $\Gamma_{R1} = 0.001 \hbar\omega_p$ ,  $\varepsilon_2 = 0.5 \hbar\omega_p$ ,  $\varepsilon_1 = -0.5 \hbar\omega_p$ ,  $m_{ep} = 5 \times 10^{-4} \hbar\omega_p$ ,  $\gamma_p = 1 \times 10^{-6} \hbar\omega_p$ ,  $\mu_L = 0.8 \hbar\omega_p$ , and  $k_B T = 0.1 \hbar\omega_p$ . In our calculations, we set  $e = k_B = \hbar = 1$ .

where  $n = \sum_{i=\uparrow,\downarrow} d_i^\dagger d_i$  is the total electron occupation number operator on the molecule and it has a maximum 2,  $\varepsilon_0$  is the on-site energy,  $U$  is the on-site Coulomb repulsion energy between two electrons, and  $V_{\alpha k, i}$  is the electrode-molecule coupling parameter. The Hamiltonians for  $H_p$  and  $H_b$  are the same as in model I.

To consider this model, a Lang-Firsov transformation to the polaron representation can be performed [41]. Applying the unitary operator  $D = e^{[\lambda(a_p^\dagger - a_p)n]}$  to the total Hamiltonian, we obtain

$$\begin{aligned}
 \mathcal{H}' &= D\mathcal{H}D^\dagger, \\
 \mathcal{H}'_m &= (\varepsilon_0 - m_{ep}^2 \hbar\omega_p)n + (U - 2m_{ep}^2 \hbar\omega_p)n(n-1), \\
 \mathcal{H}'_{el} &= \sum_{\alpha=L,R} \sum_k (\varepsilon_{k\alpha} - \mu_\alpha) c_{k\alpha}^\dagger c_{k\alpha} \\
 &\quad + \sum_{\alpha=L,R} \sum_k \sum_{i=\uparrow,\downarrow} (V_{\alpha k, i} e^{-\lambda m_{ep} (a_p^\dagger - a_p)} c_{k\alpha}^\dagger d_i + \text{H.c.}), \\
 \mathcal{H}'_p &= \hbar\omega_p \left( a_p^\dagger a_p + \frac{1}{2} \right), \\
 \mathcal{H}'_{ep} &= 0, \\
 \mathcal{H}'_d &= \mathcal{H}_d.
 \end{aligned} \tag{7}$$

Thus in the polaron representation, for a state  $|lm\rangle$  which indicates  $l$  electrons on the molecule with  $m$  vibrations, we get  $\mathcal{H}'|lm\rangle = E_{lm}|lm\rangle$  with eigenvalues

$$E_{lm} = \varepsilon' l + U' l(l-1) + \hbar\omega_p \left( m + \frac{1}{2} \right), \tag{8}$$

where  $\varepsilon' = \varepsilon_0 - m_{ep}^2 \hbar\omega_p$ ,  $U' = U - 2m_{ep}^2 \hbar\omega_p$ .

In fact, a generalized master equation in this case for the reduced density operator of the electron-vibration system within the Born-Markov approximation can be obtained, as shown in Eq. (2). By using the secular approximation, we can get the evolution of vibration populations (diagonal elements) and coherence (off-diagonal elements), respectively. For our case, we mainly focus on the former, resulting in a rate equation

$$\begin{aligned}
 \dot{p}_{|lm\rangle} &= \sum_{l' \neq l} \sum_{m' \neq m} [\Gamma_{(l'm')(lm)} p_{|l'm'\rangle} - \Gamma_{(lm)(l'm')} p_{|lm\rangle}] \\
 &\quad + m\gamma_p n_B p_{|l(m-1)\rangle} + (m+1)\gamma_p (1 + n_B) p_{|l(m+1)\rangle} \\
 &\quad - [(m+1)\gamma_p n_B + m\gamma_p (1 + n_B)] p_{|lm\rangle},
 \end{aligned} \tag{9}$$

where  $p_{|lm\rangle}$  is the probability that the system is in the  $|lm\rangle$  state,  $\Gamma_{(lm)(l'm')}$  is the probability that the system evolves from

$|lm\rangle$  to  $|l'm'\rangle$ , and

$$\Gamma_{(l_< m)(l_> m')} = |M_{mm'}|^2 \sum_{\alpha=L,R} \Gamma_{\alpha} f_{\alpha}(E_{l_> m'} - E_{l_< m}) \delta_{l_> -l_<, 1},$$

$$\Gamma_{(l_> m)(l_< m')} = |M_{mm'}|^2 \sum_{\alpha=L,R} \Gamma_{\alpha} [1 - f_{\alpha}(E_{l_> m} - E_{l_< m'})] \delta_{l_> -l_<, 1},$$
(10)

where  $l_> > l_<$ , and  $|M_{mm'}|^2$  is the Franck-Condon matrix element that is presented in Appendix B.

By applying the steady-state condition  $\dot{p}_{lm} = 0$  to the rate equations, we can calculate the probability  $p_{|lm\rangle}$ . By calculating the net electron transition probability between the left electrode and the molecule, we can obtain the steady-state current

$$I = e \sum_{l,m} \sum_{\substack{l' \neq l, \\ m' \neq m}} s \Gamma'_{(lm)(l'm')} p_{|lm\rangle},$$
(11)

where the direction of the current is from the lower chemical potential side to the higher side,  $e$  is the elementary charge, and  $s = \pm 1$  determined by the electronic tunneling direction for a given electron transition. When an electron tunnels from the higher chemical potential side to the lower side,  $s = -1$ , otherwise  $s = 1$ .  $\Gamma'_{(lm)(l'm')}$  is a part of  $\Gamma_{(lm)(l'm')}$ , which gives the probability of a state transition from  $|lm\rangle$  to  $|l'm'\rangle$  induced by electron tunneling between the left electrode and the molecule.

### C. Characteristic vibrational quantities

We use several physical quantities to characterize the properties of a vibrational state, including the average population, the effective temperature, the thermal entropy, the von Neumann entropy, and the vibration second-order coherence function. For this we write the probability of the system with  $m$  vibrational quanta as  $p_m$ , then  $p_m = p_{m,m}$  for model I, and  $p_m = \sum_l p_{|lm\rangle}$  for model II. The average population  $\langle n \rangle$  can be defined as

$$\langle n \rangle = \sum_m m p_m.$$
(12)

Given  $\langle n \rangle$ , if we assume that the vibration is in thermal equilibrium, we can define an effective temperature  $T_{\text{eff}}$  as

$$T_{\text{eff}} = \frac{\hbar\omega_p/k_B}{\ln(1/\langle n \rangle + 1)}.$$
(13)

Consequently, we can define the effective thermal entropy  $S_{\text{th}}$  as

$$S_{\text{th}} = k_B [(\langle n \rangle + 1) \ln(\langle n \rangle + 1) - \langle n \rangle \ln \langle n \rangle].$$
(14)

By comparing  $S_{\text{th}}$  with the actual von Neumann entropy

$$S_{\text{vN}} = -k_B \sum_m p_m \ln p_m,$$
(15)

we can characterize the deviation from the thermal state. Alternatively, the Kullback-Leibler divergence can also measure the deviation, which is defined as

$$D_{\text{KL}} = \sum_m q_m \ln \left( \frac{q_m}{p_m} \right),$$
(16)

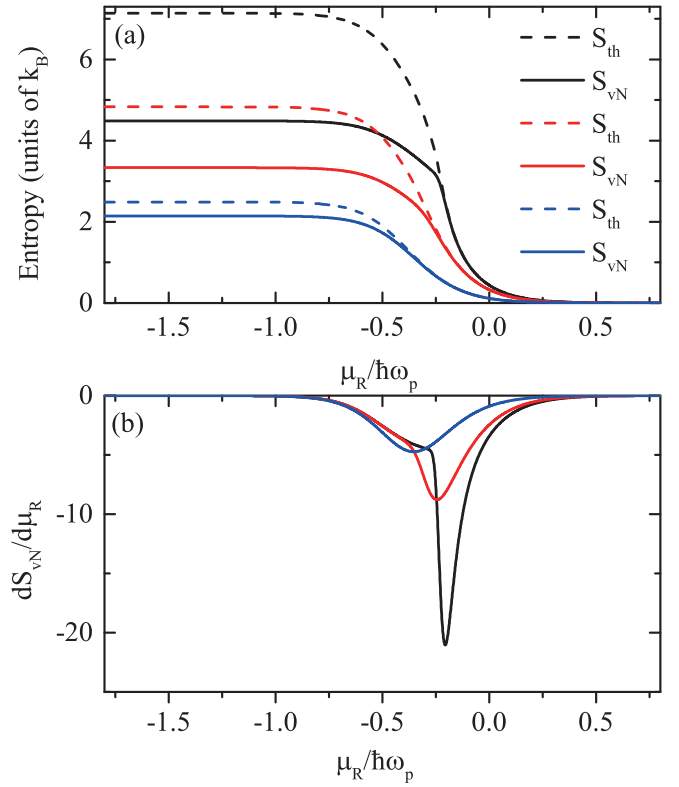


FIG. 3. Entropy  $S_{\text{th}}$  and  $S_{\text{vN}}$  as a function of the chemical potential of the right electrode  $\mu_R$  with  $\mu_L = 0.8 \hbar\omega_p$ . The lines (black, red, blue) are plotted for three different values of  $\gamma_p$  ( $10^{-6}$ ,  $10^{-5}$ ,  $10^{-4}$ )  $\hbar\omega_p$ . (b) The corresponding differential spectra of  $S_{\text{vN}}$  in (a).

where  $q_m$  represents the thermal distribution and has a Boltzmann form

$$q_m = e^{-m\hbar\omega_p/k_B T_{\text{eff}}} (1 - e^{-\hbar\omega_p/k_B T_{\text{eff}}}).$$
(17)

Another quantity we can use to quantify the nonthermal state is the vibrational second-order coherence function

$$g^{(2)}(0) = \frac{\langle a_p^\dagger a_p^\dagger a_p a_p \rangle}{\langle a_p^\dagger a_p \rangle^2} = \frac{\sum_m m(m-1) p_m}{(\sum_m m p_m)^2}.$$
(18)

It has been widely used in quantum optics. One can easily verify that the vibration in thermal equilibrium yields  $g^{(2)}(0) = 2$ . When  $g^{(2)}(0) < 1$ , the vibration is in the antibunching state, while for  $g^{(2)}(0) > 1$  it is in the bunching state. Thus, vibrations are bunched in the thermal state due to its bosonic statistics. Moreover, when  $g^{(2)}(0) = 1$  the vibration is in the coherent state.

## III. RESULTS AND DISCUSSIONS

### A. Results for model I

Let us begin with the case of a two-level molecular junction shown in Fig. 1(a). The higher level  $\varepsilon_2$  couples only to the left electrode, and the lower level  $\varepsilon_1$  couples only to the right electrode, that is,  $\Gamma_{R1} \neq 0$ ,  $\Gamma_{L2} \neq 0$ , while  $\Gamma_{R2} = \Gamma_{L1} = 0$ . Such a model has been used before to study resonant vibration excitation [25,33–35,42–44]. The vibration in such a junction is excited by the inelastic electron tunneling from level 2 to

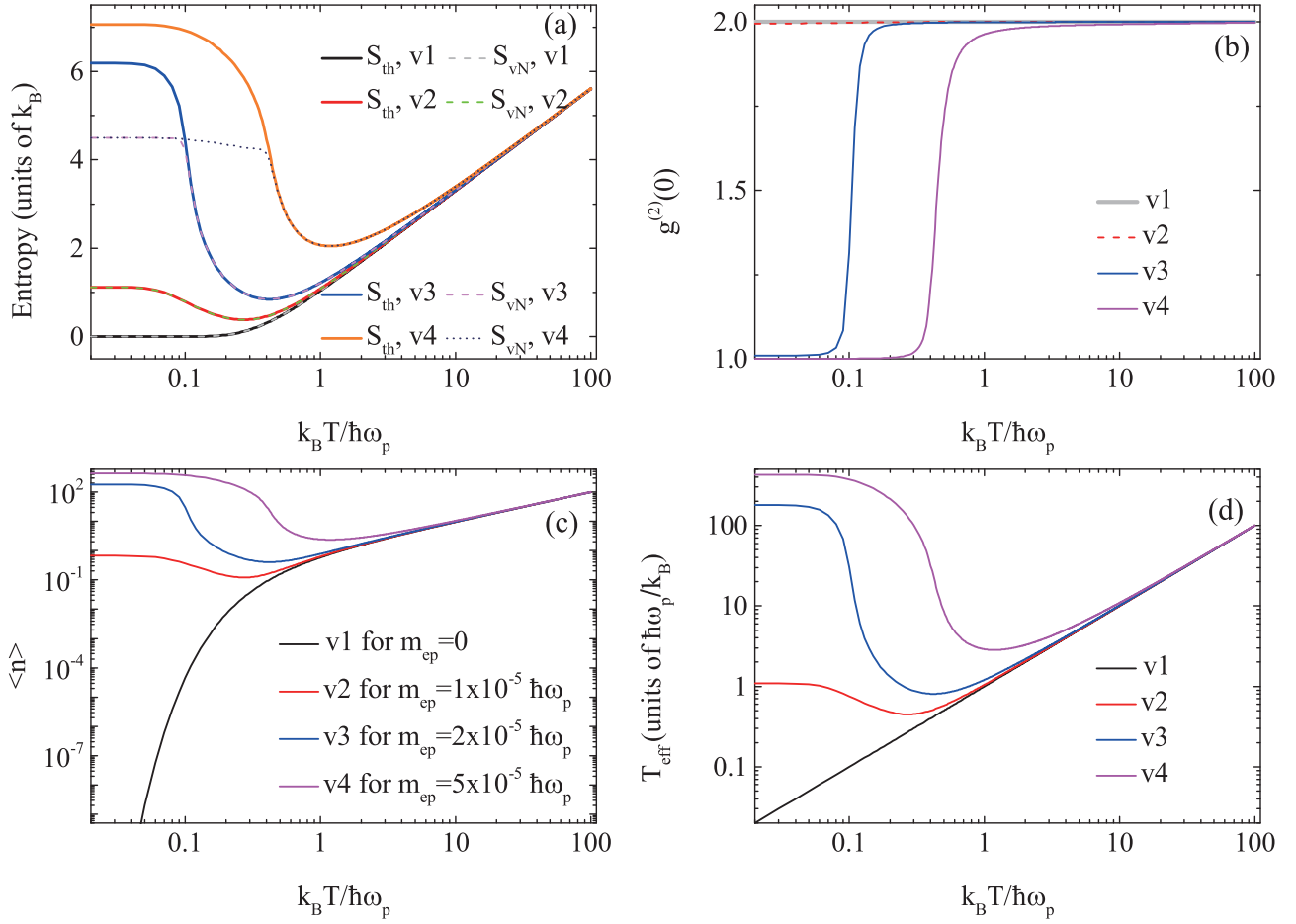


FIG. 4. Effect of temperature on vibration statistics for various values of  $m_{ep}$  at  $\mu_R = -0.8 \hbar\omega_p$ . (a) The entropy  $S_{th}$  and  $S_{vN}$ , (b) the second-order coherence function  $g^{(2)}(0)$ , (c) the effective temperature  $T_{eff} = T$ , and (d) the average population  $\langle n \rangle$  as a function of the temperature  $k_B T$ . The other parameters are the same as in Fig. 2.

level 1. We set the Coulomb repulsion inside the molecule  $U_{12} = \infty$ . The Lindblad master equation in Sec. II A is used to obtain the following results.

### 1. Bias dependence of the vibrational state

In Fig. 2(a), the effective temperature  $T_{eff}$  and the average population  $\langle n \rangle$  are plotted as a function of the chemical potential of the right electrode  $\mu_R$  with fixed  $\mu_L = 0.8 \hbar\omega_p$ . As we can see, the magnitudes of  $T_{eff}$  and  $\langle n \rangle$  decrease with increasing  $\mu_R$  from  $-1.8 \hbar\omega_p$  to  $0.8 \hbar\omega_p$ . The reason is as follows. By adjusting  $\mu_R$  [the inset in Fig. 2(a)], we can get two electron transport regimes and vibration statistics. For  $\mu_R < \varepsilon_1$ , the electron in the left electrode can tunnel to level 2 and relax to level 1, accompanied by emission of a vibration. The electron in level 1 can tunnel to the right electrode afterward. For  $\mu_R > \varepsilon_1$ , the inelastic transition is blocked because level 1 is always populated by one electron from the right electrode. Due to the strong Coulomb interaction, no electron can be injected from the left electrode to level 2, such that no vibration can be excited. In such a case,  $T_{eff}$  reduces to the temperature of the vibration bath; see the dashed line in Fig. 2(a).

A similar analysis using effective temperature has been performed in previous studies [11,28,29,32,45–51]. Here, we

go one step further and compare the thermal  $S_{th}$  and the von Neumann entropy  $S_{vN}$  to characterize the deviation of the vibration from the thermal state. The difference of the entropy  $\Delta S = S_{th} - S_{vN}$  indicates the nonequilibrium nature of the steady state. When they differ from each other, it is not enough to describe the vibrational state with a single effective temperature. As expected, we observe this situation in Fig. 2(b). For example, when  $\mu_R < \varepsilon_1$ , the population inversion between levels 2 and 1 leads to a vibrational lasing situation. The lasing threshold is located at  $\mu_R = \varepsilon_1$ . Above the threshold ( $\mu_R < \varepsilon_1$ ), the vibration statistics obey Poisson distribution and  $S_{th} \neq S_{vN}$  [Fig. 2(c)]. Below the threshold ( $\mu_R > \varepsilon_1$ ), the vibration reaches the thermal state, where  $p_m$  follows a Boltzmann distribution [Fig. 2(d)] and  $S_{th} = S_{vN}$ . Therefore, a single effective temperature is only suitable for describing thermal vibrations below the threshold.

It is worth pointing out that a kink near the lasing transition in the red curve of Fig. 2(b) can be observed. To clarify this, we plot entropy  $S_{th}$  and  $S_{vN}$  as a function of the chemical potential  $\mu_R$  for more values of  $\gamma_p$  in Fig. 3(a). The curves in Fig. 2(b) are reproduced. It seems that the kink is a characteristic property of the lasing transition. It is more obvious for small coupling to the vibrational bath and is broadened out for larger coupling.

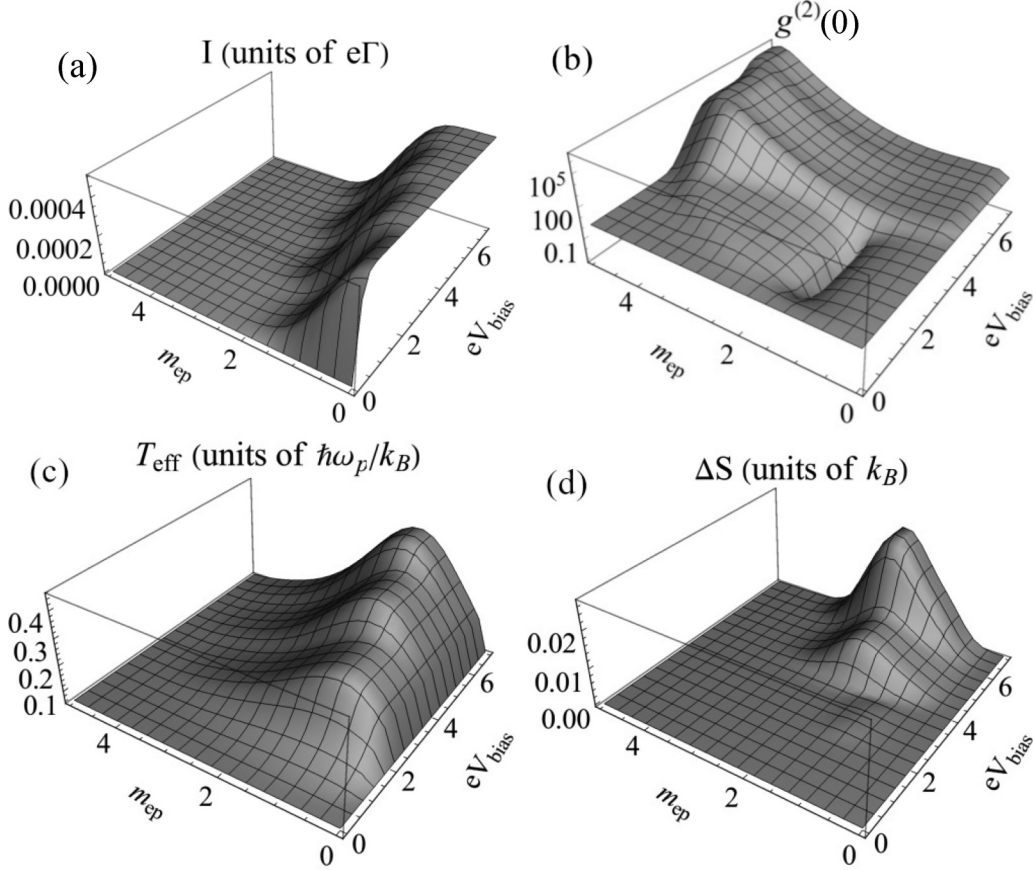


FIG. 5. 3D plot of the current  $I$  (a), the second-order coherence function  $g^{(2)}(0)$  (b), the effective temperature  $T_{eff}$  (c), and the entropy difference  $\Delta S$  (d) as functions of the voltage bias  $V_{bias}$  and electron-vibration coupling constant  $m_{ep}$  (both units of  $\hbar\omega_p$ ). A symmetric voltage drop is applied to the two electrodes. Other parameters are  $\varepsilon' = 0$ ,  $\Gamma_L = \Gamma_R = \Gamma = 1 \times 10^{-3} \hbar\omega_p$ ,  $k_B T = 0.06 \hbar\omega_p$ ,  $U' = \infty$ , and  $\gamma_p = 0.01 \hbar\omega_p$ .

## 2. Vibration thermalization

We now consider the effect of temperature on vibration statistics; see Fig. 4. Above, we have analyzed the range of  $k_B T \ll \hbar\omega_p$ . The difference between the thermal entropy and the von Neumann entropy indicates that the effective temperature is not applicable at  $\mu_R < \varepsilon_1$  (above the threshold of laser), while for  $k_B T \gg \hbar\omega_p$  and  $\mu_R < \varepsilon_1$ , one may expect  $S_{th} = S_{vN}$ , as shown in Fig. 4(a). This is a consequence of thermalization of the vibrational mode due to the coupling with a high-temperature vibration bath. To show the crossover of the vibration statistics from low temperature to high temperature more explicitly, in Fig. 4(b) we present the temperature dependence of the second-order coherence function  $g^{(2)}(0)$ . This clearly shows the transitions of the vibration state from coherent to thermal, corresponding to  $g^{(2)}(0) = 1$  to  $g^{(2)}(0) = 2$ . This again shows that the effective temperature is suitable for describing thermal vibrations, but not for coherent vibrations.

We notice that the entropy, the average population, and the effective temperature do not change monotonically with increasing temperature  $k_B T$  when  $m_{ep} \neq 0$ . They drop down in the region  $[0.1, 1] k_B T / \hbar\omega_p$ . This nonmonotonous behavior is due to the vibrational decay through inelastic electronic excitation of electron-hole pairs. At zero temperature, the upper level  $\varepsilon_2$  is filled and the lower level  $\varepsilon_1$  is empty. This perfect population inversion prohibits vibrational decay to the

electronic system. With increasing temperature, due to the broadening of the Fermi distribution, the population of level  $\varepsilon_2$  is less than 1 and that of level  $\varepsilon_1$  is larger than zero. Vibrational decay through electron excitation at level  $\varepsilon_1$  to level  $\varepsilon_2$  becomes possible. This serves as a decay channel for the vibrational mode, leading to an initial decrease in Figs. 4(a), 4(c), and 4(d).

Figures 2–4 are the first main result of this work, showing that the vibration coupled weakly to an electron can reach a thermal or coherent state, and that one effective temperature is not enough to describe such a state. A different way to demonstrate the effective temperature is to consider the strong electron-vibration coupling, which can excite nonthermal vibrations other than the coherent states. We will discuss the nature and origin of such nonthermal vibrations in the next section.

## B. Results for model II

Now we consider the single-level model in Fig. 1(b). The rate equation is applied under the polaron representation by using the Lang-Firsov transformation, as discussed in Sec. II B. Figure 5 summarizes the dependence of  $T_{eff}$ , the difference between  $S_{th}$  and  $S_{vN}$  [defined as  $\Delta S = (S_{th} - S_{vN})$ ] and  $g^{(2)}(0)$  on the voltage bias  $V_{bias}$  and  $m_{ep}$ . Figure 6 shows

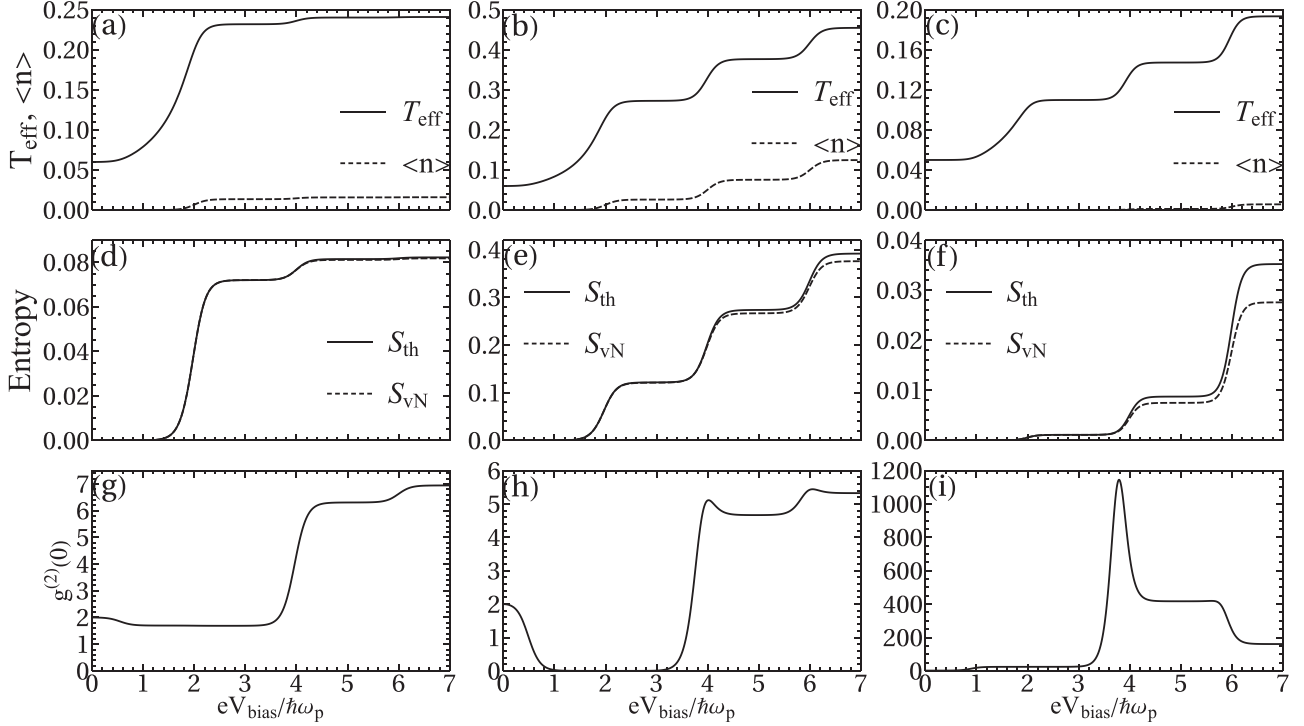


FIG. 6. The effective temperature  $T_{\text{eff}}$  (units of  $\hbar\omega_p/k_B$ ) [solid lines in (a)–(c)], the average vibration occupation  $\langle n \rangle$  [dashed lines in (a)–(c)], the effective thermal entropy  $S_{vN}$  [solid lines in (d)–(f)], the von Neumann entropy  $S_{\text{th}}$  (units of  $k_B$ ) [dashed lines in (d)–(f)], and the second-order coherence function  $g^{(2)}(0)$  in (g)–(i) vs the voltage bias  $V_{\text{bias}}$ , where  $m_{ep} = 0.4 \hbar\omega_p$ ,  $m_{ep} = 1.4 \hbar\omega_p$ , and  $m_{ep} = 3 \hbar\omega_p$  is calculated in the first, second, and third row. The other parameters are the same as in Fig. 5.

the line plots of their values for representative values of  $m_{ep}$  for weak, medium, and strong couplings.

At low electron-vibration coupling ( $m_{ep} = 0.4 \hbar\omega_p$ ), the single vibration emission process is dominant; see  $T_{\text{eff}}$  and  $\langle n \rangle$  in Fig. 6(a). There is no obvious difference between  $S_{vN}$  and  $S_{\text{th}}$ , especially in the low bias region [Fig. 6(c)]. Consequently, the effective temperature works very well. When the electron vibration is increased ( $m_{ep} = 1.4 \hbar\omega_p$ ), multivibration excitation becomes possible and Franck-Condon steps appear [Fig. 6(b)]. Antibunching among emitted vibrations [ $g^{(2)}(0) < 1$ ] can be observed near the first Franck-Condon step ( $eV_{\text{bias}} = \hbar\omega_p$ ), which has been discussed in detail in Ref. [52]. In this regime, single vibration emission dominates. Thus,  $S_{vN}$  and  $S_{\text{th}}$  still coincide with each other. The difference between  $S_{vN}$  and  $S_{\text{th}}$  becomes obvious at larger bias [Fig. 6(e)]. Further increasing  $m_{ep}$  leads to larger deviation between the two entropies at high bias [Fig. 6(f)]. Comparing different cases, we find that the deviation from the thermal state characterized by  $\Delta S = S_{\text{th}} - S_{vN}$  happens at large  $V_{\text{bias}}$  and high  $m_{ep}$ , when the multivibration excitation process becomes important. In this case, the vibrations show superbunching with huge  $g^{(2)}(0)$ .

On the other hand, as shown in Fig. 5, the change of  $g^{(2)}(0)$ ,  $T_{\text{eff}}$ , and  $\eta$  with  $m_{ep}$  is not monotonic. To further investigate this effect, we show the  $m_{ep}$  dependence of these quantities at a given bias  $eV_{\text{bias}} = 7 \hbar\omega_p$  in Fig. 7. This corresponds to line cuts of the three-dimensional (3D) plot. In Fig. 7(a), we can find that the current is significantly suppressed as  $m_{ep}$  increases. This can be attributed to the Franck-Condon blockade, which has been discussed in Ref. [53]. As shown

in Fig. 10 of Appendix B, when  $m_{ep} = 0.4 \hbar\omega_p$ , maximum of the Franck-Condon matrix elements is near the diagonal part where the difference in vibrational occupation number between initial and final states is small. As  $m_{ep}$  increases, the maximum moves away from the diagonal. A higher occupation number difference needs higher excitation energy and consequently larger voltage bias. For fixed voltage bias, increasing  $m_{ep}$  results in current suppression. For  $T_{\text{eff}}$  or  $\langle n \rangle$  in Fig. 7(b), there exists a maximum at an intermediate value of  $m_{ep} \sim 1.4 \hbar\omega_p$ . The reason is as follows. For one limit  $m_{ep} = 0$ , there is no vibration excitation, such that  $T_{\text{eff}} = T$  and  $\langle n \rangle \approx 0$ . For the other limit with large  $m_{ep}$ , a Franck-Condon blockade leads to the suppression of vibration excitation, again resulting in  $T_{\text{eff}} = T$  and  $\langle n \rangle \approx 0$ . Thus, there exists a maximum between the two limits. Similar behavior is found for the entropy [Fig. 7(c)]:  $S_{vN} = S_{\text{th}} \approx 0$  for  $m_{ep} \ll \hbar\omega_p$  and  $m_{ep} \gg \hbar\omega_p$ , corresponding to thermal vibrations [see also  $g^{(2)}(0)$  in Fig. 7(d)]. The basic features of  $\Delta S$  are similar to those of  $S_{\text{th}}$  and  $S_{vN}$ . The maximum of  $\Delta S$  moves to larger  $m_{ep}$  compared to  $T_{\text{eff}}$  or  $\langle n \rangle$ . We also calculate the Kullback-Leibler divergence  $D_{\text{KL}}$  according to Eq. (16), which can measure the degree to which the vibration deviates from equilibrium. It is found that the changes of  $D_{\text{KL}}$  and  $\Delta S$  with  $m_{ep}$  are consistent. Moreover, we present the statistical distribution of different vibrational states when  $\Delta S$  takes the maximum value in Fig. 8, where deviation from the Boltzmann distribution can be clearly seen.

Up to this point, we considered the strong Coulomb interaction with  $U' = \infty$ , where no more than one electron can reside on the molecule. For  $U' < eV_{\text{bias}}$ , one may expect

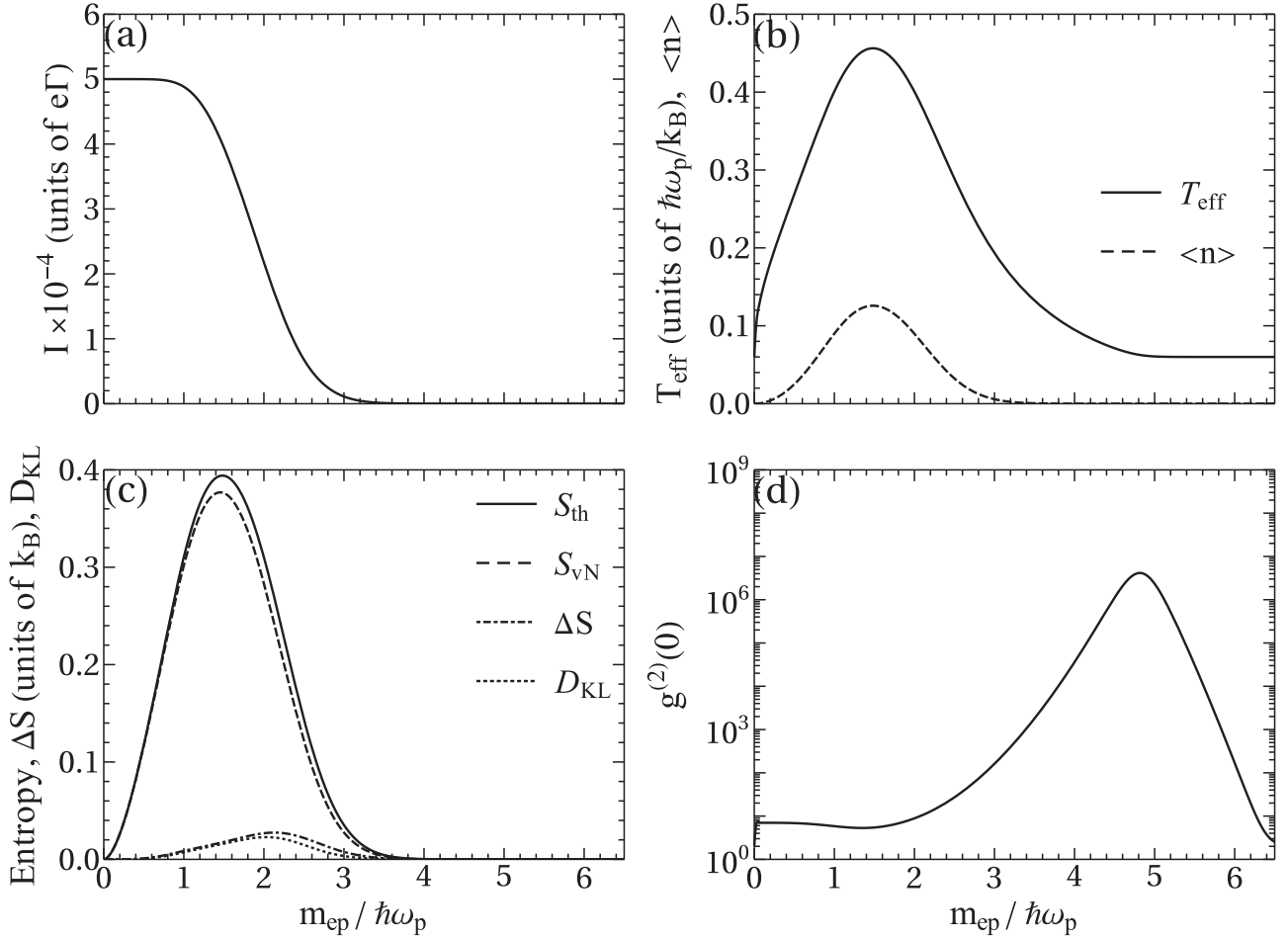


FIG. 7. (a) The current  $I$  vs as a function of the electron-vibration coupling strength  $m_{ep}$ . (b) The effective temperature  $T_{\text{eff}}$  and the average vibration occupation  $\langle n \rangle$  vs  $m_{ep}$ . (c) The effective thermal entropy  $S_{\text{vN}}$ , the von Neumann entropy  $S_{\text{th}}$ , the entropy difference  $\Delta S$ , and the Kullback-Leibler divergence  $D_{\text{KL}}$  vs  $m_{ep}$ . (d) The second-order coherence function  $g^{(2)}(0)$  vs  $m_{ep}$ . The applied bias is taken as  $eV_{\text{bias}} = 7\hbar\omega_p$ . The other parameters are the same as in Fig. 5.

more than one electron to participate in the transport at the same time. Therefore, we show the effect of the Coulomb interaction on the vibration statistics in Fig. 9. We find

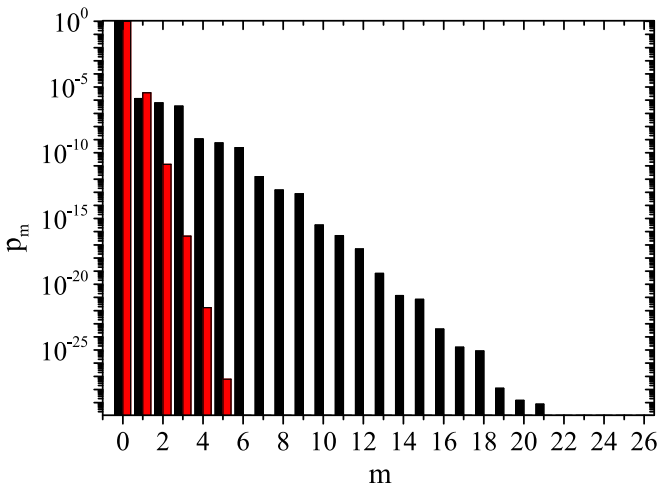


FIG. 8. Vibration statistics when  $\Delta S$  reaches a maximum as in Fig. 7(c). The red histogram is obtained from Eq. (17).

additional Coulomb blockade steps in the results. Although  $\Delta S$  changes at Coulomb blockade steps, the overall change is quite small and does not change much with  $U'$  in the weak electron-vibration coupling regime.

### C. Discussions

Energy dissipation in molecular junction has received considerable attention in the past years. It is normally termed Joule heating, although subsequent studies show that, in addition to stochastic Joule heating, electrical current can also do deterministic work on the nuclei. The effective temperature has been widely used to quantify the nonequilibrium steady state of vibrations. Our results in this work show that a single effective temperature cannot always fully describe this vibrational steady state. We show that the difference between the effective thermal entropy  $S_{\text{th}}$  and the actual von Neumann entropy  $S_{\text{vN}}$  can be used to quantify the deviation from the thermal state.

Since the thermal entropy is always larger than the actual entropy, their difference  $\Delta S$  can be used to characterize the nonequilibrium nature of the vibrational steady state. More importantly,  $\Delta S > 0$  implies that the nonequilibrium free



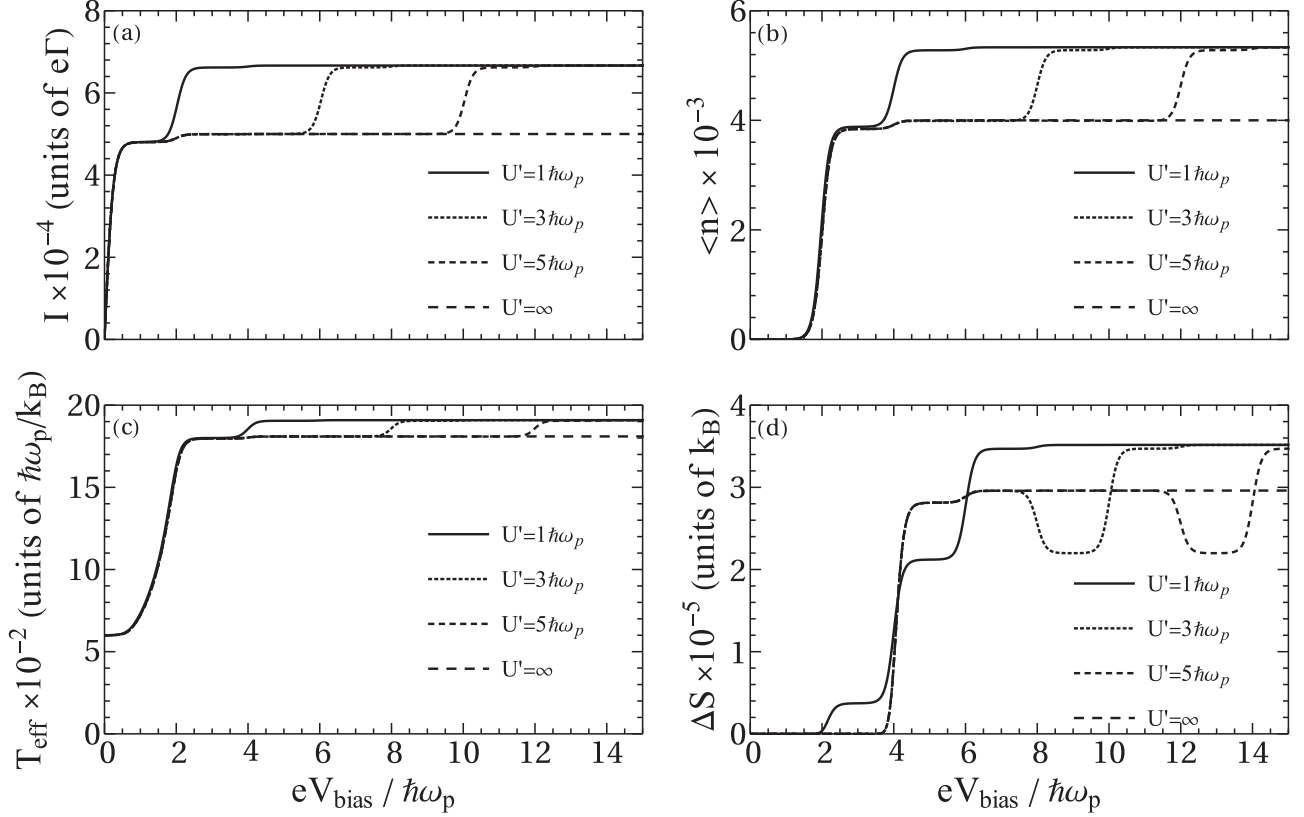


FIG. 9. The current  $I$  (a), the average vibration occupation  $\langle n \rangle$  (b), the effective temperature  $T_{\text{eff}}$  (c), and entropy difference  $\Delta S$  (d) as a function of the bias  $V_{\text{bias}}$  for indicated values of the Coulomb interaction  $U'$  at  $m_{ep} = 0.2\hbar\omega_p$ . The other parameters are the same as in Fig. 5.

energy  $F = U - TS_{\text{vN}} > F_{\text{th}}$ , where  $U$  is the internal energy of the vibrational degrees of the system. Thus, this extra free energy  $\Delta F = U - F_{\text{th}}$  can be used, at least in principle, freely in carefully designed thermodynamic processes. If one were to use only the effective temperature to characterize the vibrational state, one could get results that violate the second law of thermodynamics, i.e., a Carnot engine with efficiency larger than the Carnot efficiency. This, of course, does not violate the second law, since the vibration is not in thermal equilibrium. The nonthermal statistical distribution is an extra resource that can be used to perform work.

#### IV. CONCLUSIONS

In conclusion, we have presented an analysis of the vibration statistics in biased molecular junctions. By using the Lindblad master equation, a two-level molecular system with weak electron-vibration coupling was studied. It is found that the vibrational steady states before and after the lasing threshold bias are different in nature. The former can be well described by a single effective temperature, while in the latter case the vibration is in a coherent state, and an additional quantity  $\Delta S$  is needed to quantify its nonequilibrium property. We also considered a single-level coupling to one vibrational mode in the Holstein form. The rate equation with Lang-Firsov transformation is used to study the vibration statistics. The results indicate that for large electron-vibration coupling

and high bias, similar to the lasing situation in the two-level model, multivibration emission leads to a nonequilibrium state with lower entropy and thus higher free energy. These results show that the vibration mode in biased molecular junctions cannot always be characterized by a single effective temperature. The nonequilibrium vibrations may be utilized in carefully designed thermodynamic machines to achieve higher efficiencies. We considered molecular junctions in this work, but our model can be easily extended and applied to artificial molecules, i.e., quantum dot systems.

#### ACKNOWLEDGMENTS

This work is supported by the National Natural Science Foundation of China (Grant No. 21873033), the National Key Research and Development Program of China (Grant No. 2017YFA0403501), and the program for HUST academic frontier youth team. L.-L.N. acknowledges support from the China Postdoctoral Science Foundation (Grant No. 2020M672322).

#### APPENDIX A: MATRIX ELEMENTS OF THE DENSITY OPERATOR

The matrix elements of the electron-vibration density operator  $\rho$  can be defined as

$$\rho_{m,n}^{ij} := \langle m, i | \rho | j, n \rangle, \quad (\text{A1})$$

where  $i, j = 0, g, e$  and  $m/n$  is the vibration Fock state. Then, we can get the matrix elements

$$\begin{aligned} \dot{\rho}_{m,n}^{00} = & -i\omega_p(m-n)\rho_{m,n}^{00} - (\Gamma_{L1}^f + \Gamma_{R1}^f + \Gamma_{L2}^f + \Gamma_{R2}^f)\rho_{m,n}^{00} + (\Gamma_{L1}^{fo} + \Gamma_{R1}^{fo})\rho_{m,n}^{gg} + (\Gamma_{L2}^{fo} + \Gamma_{R2}^{fo})\rho_{m,n}^{ee} \\ & + \frac{\gamma_p}{2}n_B[2\sqrt{m}\sqrt{n}\rho_{m-1,n-1}^{00} - (m+n+2)\rho_{mn}^{00}] + \frac{\gamma_p}{2}(n_B+1)[2\sqrt{m+1}\sqrt{n+1}\rho_{m+1,n+1}^{00} - (m+n)\rho_{mn}^{00}], \end{aligned} \quad (A2)$$

$$\begin{aligned} \dot{\rho}_{m,n}^{gg} = & -i\omega_p(m-n)\rho_{m,n}^{gg} + (\Gamma_{L1}^f + \Gamma_{R1}^f)\rho_{m,n}^{00} - (\Gamma_{L1}^{fo} + \Gamma_{R1}^{fo})\rho_{m,n}^{gg} - im_{ep}(\sqrt{m}\rho_{m-1,n}^{eg} - \sqrt{n}\rho_{m,n-1}^{ge}) \\ & + \frac{\gamma_p}{2}n_B[2\sqrt{m}\sqrt{n}\rho_{m-1,n-1}^{gg} - (m+n+2)\rho_{mn}^{gg}] + \frac{\gamma_p}{2}(n_B+1)[2\sqrt{m+1}\sqrt{n+1}\rho_{m+1,n+1}^{gg} - (m+n)\rho_{mn}^{gg}], \end{aligned} \quad (A3)$$

$$\begin{aligned} \dot{\rho}_{m,n}^{ee} = & -i\omega_p(m-n)\rho_{m,n}^{ee} + (\Gamma_{L2}^f + \Gamma_{R2}^f)\rho_{m,n}^{00} - (\Gamma_{L2}^{fo} + \Gamma_{R2}^{fo})\rho_{m,n}^{ee} - im_{ep}(\sqrt{m+1}\rho_{m+1,n}^{ge} - \sqrt{n+1}\rho_{m,n+1}^{eg}) \\ & + \frac{\gamma_p}{2}n_B[2\sqrt{m}\sqrt{n}\rho_{m-1,n-1}^{ee} - (m+n+2)\rho_{mn}^{ee}] + \frac{\gamma_p}{2}(n_B+1)[2\sqrt{m+1}\sqrt{n+1}\rho_{m+1,n+1}^{ee} - (m+n)\rho_{mn}^{ee}], \end{aligned} \quad (A4)$$

$$\begin{aligned} \dot{\rho}_{m,n}^{se} = & -i\omega_p(m-n)\rho_{m,n}^{se} - im_{ep}(\sqrt{m}\rho_{m-1,n}^{ee} - \sqrt{n+1}\rho_{m,n+1}^{gg}) + i(\varepsilon_l - \varepsilon_h)\rho_{m,n}^{se} \\ & - \left(\frac{1}{2}\Gamma_{L1}^{fo} + \frac{1}{2}\Gamma_{R1}^{fo} + \frac{1}{2}\Gamma_{L2}^{fo} + \frac{1}{2}\Gamma_{R2}^{fo}\right)\rho_{m,n}^{se} + \frac{\gamma_p}{2}n_B[2\sqrt{m}\sqrt{n}\rho_{m-1,n-1}^{se} - (m+n+2)\rho_{mn}^{se}] \\ & + \frac{\gamma_p}{2}(n_B+1)[2\sqrt{m+1}\sqrt{n+1}\rho_{m+1,n+1}^{se} - (m+n)\rho_{mn}^{se}], \end{aligned} \quad (A5)$$

$$\begin{aligned} \dot{\rho}_{m,n}^{eg} = & -i\omega_p(m-n)\rho_{m,n}^{eg} - im_{ep}(\sqrt{m+1}\rho_{m+1,n}^{gg} - \sqrt{n}\rho_{m,n-1}^{ee}) - i(\varepsilon_l - \varepsilon_h)\rho_{m,n}^{eg} \\ & - \left(\frac{1}{2}\Gamma_{L1}^{fo} + \frac{1}{2}\Gamma_{R1}^{fo} + \frac{1}{2}\Gamma_{L2}^{fo} + \frac{1}{2}\Gamma_{R2}^{fo}\right)\rho_{m,n}^{eg} + \frac{\gamma_p}{2}n_B[2\sqrt{m}\sqrt{n}\rho_{m-1,n-1}^{eg} - (m+n+2)\rho_{mn}^{eg}] \\ & + \frac{\gamma_p}{2}(n_B+1)[2\sqrt{m+1}\sqrt{n+1}\rho_{m+1,n+1}^{eg} - (m+n)\rho_{mn}^{eg}], \end{aligned} \quad (A6)$$

where

$$\begin{aligned} \Gamma_{Li}^f &= \Gamma_{Li}f_L(\varepsilon_i), \\ \Gamma_{Ri}^f &= \Gamma_{Ri}f_R(\varepsilon_i), \\ \Gamma_{Li}^{fo} &= \Gamma_{Li}[1 - f_L(\varepsilon_i)], \\ \Gamma_{Ri}^{fo} &= \Gamma_{Ri}[1 - f_L(\varepsilon_i)], \quad i = 1, 2. \end{aligned} \quad (A7)$$

Here,  $f_\alpha(\varepsilon_i) = 1/[e^{(\varepsilon_i - \mu_\alpha)/k_B T} + 1]$  is the Fermi-Dirac distribution of electrode  $\alpha$  with the chemical potential  $\mu_\alpha$  and the temperature  $T$ . Note that we limit our study to the vibration laser driven by the bias voltage, such that we take  $\gamma_p$  and  $m_{ep}$  much smaller than the molecule-electrode coupling  $\Gamma_{\alpha i}$  [43,54].

## APPENDIX B: FRANCK-CONDON MATRIX ELEMENTS

The wave function of vibration state  $|n\rangle$  is given by the  $n$ th harmonic-oscillator wave function

$$\phi_n(x) = (\pi^{1/2}2^n n! l_{\text{osc}})^{-1/2} e^{-x^2/(2l_{\text{osc}}^2)} H_n(x/l_{\text{osc}}), \quad (B1)$$

in which  $l_{\text{osc}} = \sqrt{\frac{\hbar}{m\omega_p}}$  is the oscillator length and  $H_n$  is the Hermitian polynomials. Realizing the fact that  $e^{-\lambda(b^\dagger - b)} = e^{i\sqrt{2}\lambda l_{\text{osc}} d/dx}$ , which is the translation operator, and applying the Fermi Golden rule, the Franck-Condon matrix elements can be calculated as

$$\begin{aligned} M_{m_1 m_2} &= \langle \phi_{m_2} | e^{-\lambda(b^\dagger - b)} | \phi_{m_1} \rangle \\ &= \langle \phi_{m_2}(x) | \phi_{m_1}(x - \sqrt{2}\lambda l_{\text{osc}}) \rangle \\ &= [\text{sgn}(m_2 - m_1)]^{m_1 - m_2} \\ &\quad \times \lambda^{M-m} e^{-\lambda^2/2} \left(\frac{m!}{M!}\right)^{1/2} \mathbf{L}_m^{M-m}(\lambda^2), \end{aligned} \quad (B2)$$

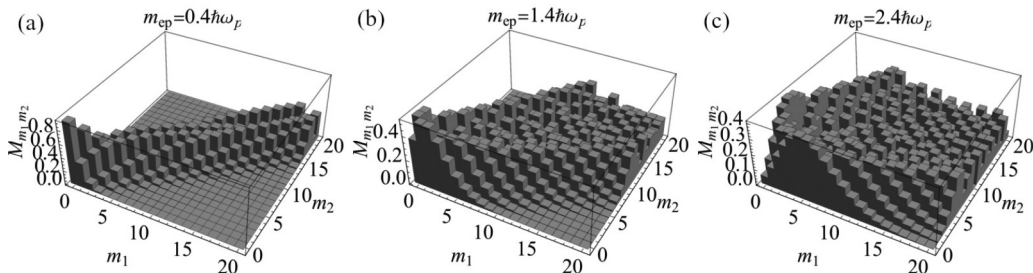


FIG. 10. The Franck-Condon elements  $M_{mm'}$  with  $m_{ep} = 0.4 \hbar\omega_p$  (a),  $m_{ep} = 1.4 \hbar\omega_p$  (b), and  $m_{ep} = 2.4 \hbar\omega_p$  (c).

in which  $\text{sgn}(x)$  is the sign function,  $m = \min(m_1, m_2)$ ,  $M = \max(m_1, m_2)$ , and  $L_m^{M-m}(\lambda^2)$  is the generalized Laguerre polynomials. To show that the current suppression in Fig. 7(a) is

caused by the Franck-Condon blockade, in Fig. 10, we plot  $M_{mm'}$  for vibration transitions from  $m$  to  $m'$  with three different values of  $m_{ep}$ .

- 
- [1] A. Nitzan and M. A. Ratner, *Science* **300**, 1384 (2003).
- [2] A. H. Flood, J. F. Stoddart, D. W. Steuerman, and J. R. Heath, *Science* **306**, 2055 (2004).
- [3] D. Xiang, X. Wang, C. Jia, T. Lee, and X. Guo, *Chem. Rev.* **116**, 4318 (2016).
- [4] N. Xin, J. Guan, C. Zhou, X. Chen, C. Gu, Y. Li, M. A. Ratner, A. Nitzan, J. F. Stoddart, and X. Guo, *Nat. Rev. Phys.* **1**, 211 (2019).
- [5] P. Gehring, J. M. Thijssen, and H. S. van der Zant, *Nat. Rev. Phys.* **1**, 381 (2019).
- [6] M. Thoss and F. Evers, *J. Chem. Phys.* **148**, 030901 (2018).
- [7] M. A. Reed, C. Zhou, C. Muller, T. Burgin, and J. Tour, *Science* **278**, 252 (1997).
- [8] B. Stipe, M. Rezaei, and W. Ho, *Science* **280**, 1732 (1998).
- [9] L. H. Yu, Z. K. Keane, J. W. Ciszek, L. Cheng, M. P. Stewart, J. M. Tour, and D. Natelson, *Phys. Rev. Lett.* **93**, 266802 (2004).
- [10] M. Elbing, R. Ochs, M. Koentopp, M. Fischer, C. von Hänisch, F. Weigend, F. Evers, H. B. Weber, and M. Mayor, *Proc. Natl. Acad. Sci. USA* **102**, 8815 (2005).
- [11] M. Galperin, M. A. Ratner, and A. Nitzan, *J. Phys.: Condens. Matter* **19**, 103201 (2007).
- [12] A. Pecchia, G. Romano, and A. Di Carlo, *Phys. Rev. B* **75**, 035401 (2007).
- [13] H. Ness and A. J. Fisher, *Proc. Natl. Acad. Sci. USA* **102**, 8826 (2005).
- [14] J.-S. Wang, J. Wang, and J.-T. Lü, *Eur. Phys. J. B* **62**, 381 (2008).
- [15] J.-T. Lü, H. Zhou, J.-W. Jiang, and J.-S. Wang, *AIP Adv.* **5**, 053204 (2015).
- [16] Y. Dubi and M. Di Ventra, *Rev. Mod. Phys.* **83**, 131 (2011).
- [17] N. Li, J. Ren, L. Wang, G. Zhang, P. Hänggi, and B. Li, *Rev. Mod. Phys.* **84**, 1045 (2012).
- [18] D. Dundas, E. J. McEniry, and T. N. Todorov, *Nat. Nanotechnol.* **4**, 99 (2009).
- [19] J.-T. Lü, M. Brandbyge, and P. Hedegård, *Nano Lett.* **10**, 1657 (2010).
- [20] N. Bode, S. V. Kusminskiy, R. Egger, and F. von Oppen, *Phys. Rev. Lett.* **107**, 036804 (2011).
- [21] H. Park, J. Park, A. K. Lim, E. H. Anderson, A. P. Alivisatos, and P. L. McEuen, *Nature (London)* **407**, 57 (2000).
- [22] J. Gaudioso, L. J. Lauhon, and W. Ho, *Phys. Rev. Lett.* **85**, 1918 (2000).
- [23] M. Galperin, K. Saito, A. V. Balatsky, and A. Nitzan, *Phys. Rev. B* **80**, 115427 (2009).
- [24] R. Härtle and M. Thoss, *Phys. Rev. B* **83**, 115414 (2011).
- [25] L. Simine and D. Segal, *Phys. Chem. Chem. Phys.* **14**, 13820 (2012).
- [26] G. Romano, A. Gagliardi, A. Pecchia, and A. Di Carlo, *Phys. Rev. B* **81**, 115438 (2010).
- [27] R. Härtle, C. Schinabeck, M. Kulkarni, D. Gelbwaser-Klimovsky, M. Thoss, and U. Peskin, *Phys. Rev. B* **98**, 081404(R) (2018).
- [28] M. Galperin, A. Nitzan, and M. A. Ratner, *Phys. Rev. B* **75**, 155312 (2007).
- [29] Z. Huang, F. Chen, R. D'agosta, P. A. Bennett, M. Di Ventra, and N. Tao, *Nat. Nanotechnol.* **2**, 698 (2007).
- [30] D. Zhang, X. Zheng, and M. Di Ventra, *Phys. Rep.* **830**, 1 (2019).
- [31] Z. Ioffe, T. Shamai, A. Ophir, G. Noy, I. Yutsis, K. Kfir, O. Cheshnovsky, and Y. Selzer, *Nat. Nanotechnol.* **3**, 727 (2008).
- [32] D. R. Ward, D. A. Corley, J. M. Tour, and D. Natelson, *Nat. Nanotechnol.* **6**, 33 (2011).
- [33] J.-T. Lü, P. Hedegård, and M. Brandbyge, *Phys. Rev. Lett.* **107**, 046801 (2011).
- [34] G. Foti and H. Vázquez, *J. Phys. Chem. Lett.* **9**, 2791 (2018).
- [35] A. Nitzan and M. Galperin, *J. Phys. Chem. Lett.* **9**, 4886 (2018).
- [36] S. Braig and K. Flensberg, *Phys. Rev. B* **68**, 205324 (2003).
- [37] A. Mitra, I. Aleiner, and A. J. Millis, *Phys. Rev. B* **69**, 245302 (2004).
- [38] M. Galperin, A. Nitzan, and M. A. Ratner, *Phys. Rev. B* **73**, 045314 (2006).
- [39] H.-P. Breuer, F. Petruccione *et al.*, *The Theory of Open Quantum Systems* (Oxford University Press on Demand, 2002).
- [40] M. O. Scully and M. S. Zubairy, *Quantum Optics* (Cambridge University Press, Cambridge, England, 1997).
- [41] I. Lang and Y. A. Firsov, *Sov. Phys. JETP* **16**, 1301 (1963).
- [42] L. Simine and D. Segal, *J. Chem. Phys.* **138**, 214111 (2013).
- [43] N. Lambert, F. Nori, and C. Flindt, *Phys. Rev. Lett.* **115**, 216803 (2015).
- [44] B. K. Agarwalla, J.-H. Jiang, and D. Segal, *Phys. Rev. B* **92**, 245418 (2015).
- [45] Y.-C. Chen, M. Zwolak, and M. Di Ventra, *Nano Lett.* **3**, 1691 (2003).
- [46] Y.-C. Chen, M. Zwolak, and M. Di Ventra, *Nano Lett.* **5**, 621 (2005).
- [47] Z. Huang, B. Xu, Y. Chen, M. D. Ventra, and N. Tao, *Nano Lett.* **6**, 1240 (2006).
- [48] G. Schulze, K. J. Franke, A. Gagliardi, G. Romano, C. S. Lin, A. L. Rosa, T. A. Niehaus, T. Frauenheim, A. Di Carlo, A. Pecchia, and J. I. Pascual, *Phys. Rev. Lett.* **100**, 136801 (2008).
- [49] M. Tsutsui, M. Taniguchi, and T. Kawai, *Nano Lett.* **8**, 3293 (2008).
- [50] L. Arrachea, N. Bode, and F. von Oppen, *Phys. Rev. B* **90**, 125450 (2014).
- [51] J. Lykkebo, G. Romano, A. Gagliardi, A. Pecchia, and G. C. Solomon, *J. Chem. Phys.* **144**, 114310 (2016).
- [52] Q. Schaeferbeke, R. Avrieller, T. Frederiksen, and F. Pistolesi, *Phys. Rev. Lett.* **123**, 246601 (2019).
- [53] J. Koch and F. von Oppen, *Phys. Rev. Lett.* **94**, 206804 (2005).
- [54] B. K. Agarwalla, M. Kulkarni, and D. Segal, *Phys. Rev. B* **100**, 035412 (2019).